
Deep Regression for Face Alignment

Baoguang Shi^{1*} Xiang Bai¹ Wenyu Liu¹ Jingdong Wang²

¹Dept. of Electronics and Information Engineering, Huazhong Univ. of Science and Technology, China

²Microsoft Research, Beijing, China

shibaoguang@gmail.com, {xbai, liuwu}@hust.edu.cn, jingdw@microsoft.com

Abstract

In this paper, we present a deep regression approach for face alignment. The deep architecture consists of a global layer and multi-stage local layers. We apply the back-propagation algorithm with the dropout strategy to jointly optimize the regression parameters. We show that the resulting deep regressor gradually and evenly approaches the true facial landmarks stage by stage, avoiding the tendency to yield over-strong early stage regressors while over-weak later stage regressors. Experimental results show that our approach achieves the state-of-the-art performance on the benchmark datasets.

1 Introduction

Face alignment, a.k.a. facial landmark localization, is a fundamental problem in computer vision. It aims to predict landmark positions given a 2D facial image. This problem has attracted a lot of research efforts [5, 4, 26, 14, 8, 1, 16, 6]. However, it remains challenging when face images are taken under uncontrolled conditions with large variation on poses, expressions and lighting conditions.

Cascaded regression has achieved the state-of-the-art performance. Cascaded pose regression [9] and the following work explicit shape regression [3] sequentially learn a cascade of random fern regressors using shape indexed features and progressively regress the shape stage by stage over the learnt cascade. Robust cascaded pose regression [2] extends cascaded pose regression with occlusion handling, enhanced shape-indexed features and more robust initialization. Supervised descent method [25] shows that a cascade of simple linear regressors is able to achieve the superior performance. Local binary feature regression [19] speeds up the supervised descent method using the learned trees-induced binary feature representation.

We observe that the cascaded regression approach tends to learn over-strong early stage regressors but over-weak later stage regressors. The reason is that the multi-stage regressors are learnt sequentially from the first stage regressor to the last stage regressor. Inspired by the natural fact that cascaded regression is a deep neural network, we propose a deep regression approach that adopts the back-propagation algorithm with the dropout strategy to jointly optimize a deep structure. The resulting deep regressor gradually and simultaneously reduces the bias and the variance of the estimation from the first regressor to the last regressor, thus yielding a better facial landmark location. The structure illustrated in Figure 1.a consists of two sub-networks: a global layer and multi-stage local layers. The latter sub-network is the same to the structure of supervised descent method [25], and each local layer contains a local feature extraction sub-layer and a local regressor. The former sub-network aims to provide an initial result regressed from the facial image as the input of the latter local regressors.

There are some other attempts to adopt deep learning for face alignment. A cascade of three convolutional neural network (CNN) regressors [22] each of which regresses the facial landmark positions

*This work was done while the author visiting Microsoft Research, Beijing, China.

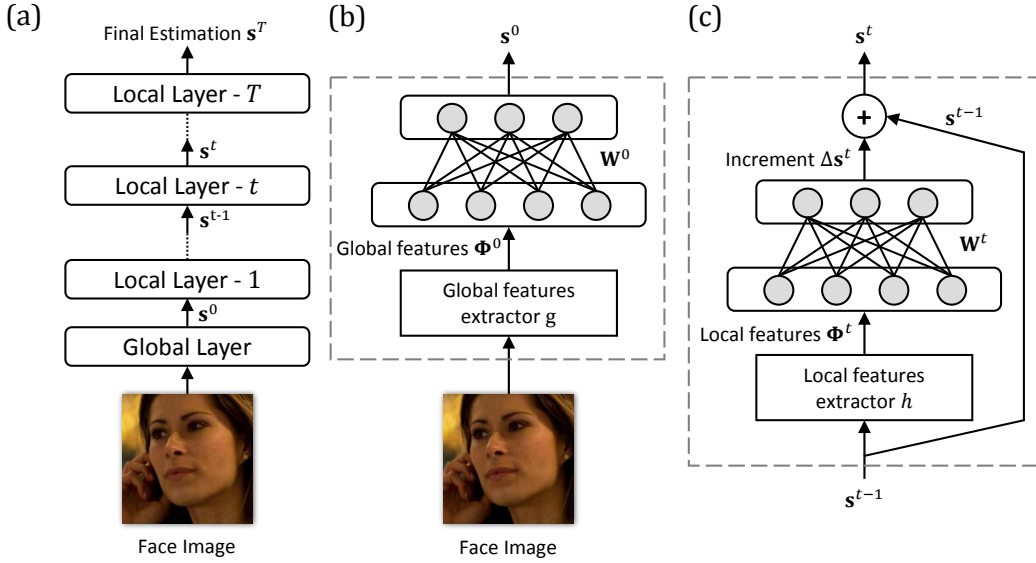


Figure 1: (a) Overview of the proposed learning architecture. The network takes face image as input and outputs shape estimation s^T . The global layer estimates initial shape s^0 and the rest local layers refine the estimation iteratively. (b) Inner structure of the global layer, see Section 2.1 for details. (c) Inner structure of the t -th local layer, see Section 2.2 for details.

is used for face alignment. Another deep learning solution, coarse-to-fine CNN cascade [27] is developed for face alignment. The two algorithms are different from our approach as all the CNNs are trained separately, in contrast our approach learns all-stage regressors jointly. In essence, the two algorithms can benefit from jointly optimizing all the three CNN regressors.

2 The Architecture

Let the vector $\mathbf{s} = [x_1, y_1, \dots, x_P, y_P]^T \in \mathbb{R}^{2P}$ be the shape of the face, where (x_p, y_p) is the position of the p -th landmark. The task of face alignment is to predict all the P landmark positions, i.e., the shape \mathbf{s} from the facial image I .

The architecture is a multi-layered deep network, depicted in Figure 1.a. The network consists of $1 + T$ layers, with the first global layer and the rest T local layers. The global layer consists of a global feature extraction layer and a global regressor. Each local layer is composed of a local feature extraction layer and a local regressor.

2.1 Global layer

The architecture of the global layer is depicted in Figure 1.b. The global layer predicts the initial shape estimation s^0 from the global feature of image I . We use linear regression for this layer and predict the initial shape s^0 directly from the global image features Φ^0 :

$$\mathbf{s}^0 = GR(I) = \mathbf{W}^0 \Phi^0 + \mathbf{b}^0, \quad \Phi^0 = g(I) \quad (1)$$

where $g(\cdot)$ extracts a d_0 -dimensional global features Φ^0 from an image, $GR(\cdot)$ represents the global regression function, $\mathbf{W}^0 \in \mathbb{R}^{2P \times d_0}$ is the linear regression coefficient matrix, and \mathbf{b}^0 is the bias vector. For clarity, the later presentation will drop this bias term in the regression function.

The linear regressor with the global feature gives a coarse estimation of the shape, which, however, is already a good initialization for the following local layers.

2.2 Local layer

Each local layer refines the shape estimated from the previous layer. The architecture of the t -th local layer is depicted in Figure 1.b. It extracts the local (shape-indexed) feature $\boldsymbol{\phi}^t$ and use it to predict the shape increment $\Delta \mathbf{s}^t$ using a linear regressor. The increment is added to \mathbf{s}^{t-1} from the previous layer to produce the refined shape estimation \mathbf{s}^t . In mathematical form:

$$\mathbf{s}^t = LR^t(I, \mathbf{s}^{t-1}) = \mathbf{s}^{t-1} + \mathbf{W}^t \boldsymbol{\phi}^t, \quad \boldsymbol{\phi}^t = h(I, \mathbf{s}^{t-1}), \quad (2)$$

where $h : I, \mathbf{s}^{t-1} \rightarrow \boldsymbol{\phi}^t \in \mathbb{R}^{d_t}$ is the local feature extraction function, $LR(\cdot, \cdot)$ represents the local regression function, $\mathbf{W}^t \in \mathbb{R}^{2P \times d_t}$ is the linear regression matrix for the t -th local regressor. $\boldsymbol{\phi}^t$ is constructed by concatenating local descriptors around each landmark: $\boldsymbol{\phi}^t = [\boldsymbol{\phi}_1^t, \boldsymbol{\phi}_2^t, \dots, \boldsymbol{\phi}_P^t]^\top$, $\boldsymbol{\phi}_p^t$ is the descriptor extracted around the p -th landmark.

Local regressors extract features that describe local appearance and is more suitable for finer adjustment of landmark positions. Besides, it uses only a subset of image pixels for feature extraction and is more advantageous on computational efficiency.

3 Optimization

The parameters in the network structure contain the regression coefficient matrices of the $(T + 1)$ regressors: $\theta = \{\mathbf{W}^0, \mathbf{W}^1, \dots, \mathbf{W}^T\}$. These parameters are learned by minimizing the objective function, $E(\theta) = \frac{1}{2} \sum_{i=1}^N \|DR^T(I_i) - \hat{\mathbf{s}}_i\|_2^2$. Here $DR^T(I_i)$ represents the output of the deep regression structure. It is written from a sequence of sub-network: $DR^T(I_i) = LR^T(I_i, DR^{T-1}(I_i))$, $DR^t(I_i) = LR^t(I_i, DR^{t-1}(I_i))$, and $DR^0(I_i) = GR(I_i)$. We first introduce a sequential learning algorithm that is used in cascaded regression [25] and empirically show the drawbacks of sequential learning. Then, we introduce the joint learning algorithm based on back-propagation.

3.1 Sequential learning

Sequential learning computes the regression coefficients one by one from \mathbf{W}^0 to \mathbf{W}^T to approximately minimize the objective function $E(\theta)$. The regression coefficient for each regressor is optimized, by fixing the trained regression coefficients of the regressors preceding it and minimizing the difference of its predicted shape from the true shape.

The coefficient matrix \mathbf{W}^0 of the global regressor is solved as

$$\mathbf{W}^0 = \underset{\mathbf{W}^0}{\operatorname{argmin}} \frac{1}{2N} \sum_{i=1}^N \|\mathbf{W}^0 \boldsymbol{\phi}_i^0 - \hat{\mathbf{s}}_i\|_2^2. \quad (3)$$

The coefficient matrix \mathbf{W}^t of the t th local regressor is solved as

$$\mathbf{W}^t = \underset{\mathbf{W}^t}{\operatorname{argmin}} \frac{1}{2N} \sum_{i=1}^N \|\mathbf{s}_i^{t-1} + \mathbf{W}^t \boldsymbol{\phi}_i^t - \hat{\mathbf{s}}_i\|_2^2, \quad (4)$$

where $\boldsymbol{\phi}_i^t = h(I_i, \mathbf{s}_i^{t-1})$ and \mathbf{s}_i^{t-1} are fixed given the coefficients of the first t regressors are estimated.

The sequential learning algorithm is clearly sub-optimal as the coefficient matrix estimation of each regressor does not exploit the later regressors. Empirically, we observe that the first few regressors make greater paces to approach the true shape, i.e., smaller bias of the shape estimation from those regressors, while the latter regressors make smaller paces. Importantly, we find that the shape estimation from the first regressors has larger estimation variances. This results in the variance of the local (shape-indexed) features is also larger. As a consequence, it is harder for the later regressors to make a good shape estimation.

In the following, we will introduce the joint learning algorithm using back-propagation to directly optimize the objective function such that the optimization of the regression coefficient matrix helps

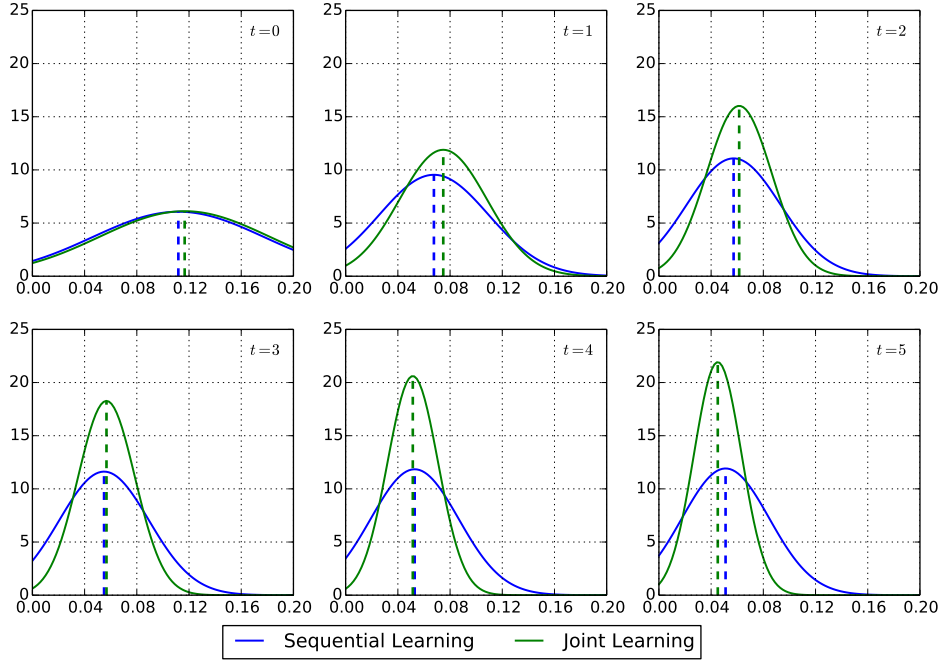


Figure 2: Bias and variance comparison of shape estimation error of each stage, learned by sequential and joint learning. Sequential learning over-strongly reduces bias early and results in larger variance (wider and shorter curve), which makes later stages weak. Joint learning balances between bias and variance and makes them gradually and simultaneously decrease, resulting in lower error eventually. The bias and variance are estimated on the 300-W Common Subset and plotted as normal distributions. x axis represents the normalized shape estimation error. (Section 4.1)

each other. The empirical results show that joint learning is able to make a balanced optimization of the bias and the variance of the shape estimation from the regressors: both the bias and the variance gradually decrease from the early regressors to the later regressors. Consequently, joint learning yields a better whole shape estimation. Figure 2 illustrates the performance comparison of each regressors using sequential learning and joint learning.

3.2 Joint learning

We adopt the gradient descent method to jointly estimate the regression coefficient matrices by minimizing the global error function $E(\theta)$. We apply the back-propagation algorithm [20] to efficiently the evaluate derivatives of the error function with respect to the coefficient matrices.

The derivatives of local layers. The partial derivatives of the error function with respect to \mathbf{W}^t and \mathbf{s}^t are computed using the backward recurrence as:

$$\frac{\partial E}{\partial \mathbf{W}^t} = \frac{\partial E}{\partial \mathbf{s}^t} \frac{\partial LR^t}{\partial \mathbf{W}^t} \quad (5)$$

$$\frac{\partial E}{\partial \mathbf{s}^{t-1}} = \frac{\partial E}{\partial \mathbf{s}^t} \frac{\partial LR^t}{\partial \mathbf{s}^{t-1}}. \quad (6)$$

According to Equation 2, $\frac{\partial E}{\partial \mathbf{W}^t} = \Phi^t \frac{\partial E}{\partial \mathbf{s}^t}$. The partial derivatives $\frac{\partial LR^t}{\partial \mathbf{s}^{t-1}}$ are computed as:

$$\frac{\partial LR^t}{\partial \mathbf{s}^{t-1}} = \mathbf{I} + \mathbf{W}^t \frac{\partial h}{\partial \mathbf{s}^{t-1}}, \quad (7)$$

where $\mathbf{I} \in \mathfrak{R}^{2P \times 2P}$ is an identity matrix, and $\frac{\partial h}{\partial \mathbf{s}^{t-1}}$ is the partial derivative of the local feature extractor with respect to the shape vector \mathbf{s}^{t-1} .

The derivatives of local feature extractors. The Jacobian matrix of the function $h(I, \mathbf{s})$ with respect to the shape \mathbf{s} is denoted by $\boldsymbol{\psi} = \frac{\partial h}{\partial \mathbf{s}}$. For simplicity, we drop the superscript t . $h(I, \mathbf{s})$ is the local feature extraction operation and is non-differentiable, and thus its gradients cannot be calculated analytically. We numerically approximate $\boldsymbol{\psi}$ by computing the second-order approximation:

$$\boldsymbol{\psi}_{ij} = \frac{\partial \Phi_i}{\partial s_j} \approx \frac{h(I, \mathbf{s}^{j+})_i - h(I, \mathbf{s}^{j-})_i}{2\epsilon}, \quad (8)$$

where \mathbf{s}^{j+} and \mathbf{s}^{j-} are equal to \mathbf{s} except the j -th dimension, where $\mathbf{s}_j^{j+} = s_j + \epsilon$ and $\mathbf{s}_j^{j-} = s_j - \epsilon$ respectively. The ϵ is chosen to be a small value which corresponds to several pixels in the image.

Since that $\boldsymbol{\Phi} = [\boldsymbol{\Phi}_1^\top, \boldsymbol{\Phi}_2^\top, \dots, \boldsymbol{\Phi}_P^\top]^\top$ is the concatenation of local descriptors extracted around P landmarks, each dimension of $\boldsymbol{\Phi}$ is determined by the corresponding landmarks positions x_p, y_p , which are two dimensions of \mathbf{s} . Therefore $\boldsymbol{\psi}$ is a block-diagonal matrix $\boldsymbol{\psi} = \text{diag}(\boldsymbol{\psi}_1, \boldsymbol{\psi}_2, \dots, \boldsymbol{\psi}_P)$ of which each block $\boldsymbol{\psi}_p = [\boldsymbol{\psi}_{px} \ \boldsymbol{\psi}_{py}]$. $\boldsymbol{\psi}_{px}$ and $\boldsymbol{\psi}_{py}$ are respectively the local descriptor gradients along the x and y axis, given by:

$$\boldsymbol{\psi}_{px} = \frac{h_p(I, x_p + \epsilon, y_p) - h_p(I, x_p - \epsilon, y_p)}{2\epsilon} \quad (9)$$

$$\boldsymbol{\psi}_{py} = \frac{h_p(I, x_p, y_p + \epsilon) - h_p(I, x_p, y_p - \epsilon)}{2\epsilon} \quad (10)$$

Here $h_p(I, x_p, y_p)$ is the local descriptor function on the p -th landmark whose coordinates are x_p, y_p .

The derivatives of the global layer. The derivatives of the error function with respect to the regression coefficient matrix \mathbf{W}^0 , according to Equation 1, are computed as follows:

$$\frac{\partial E}{\partial \mathbf{W}^0} = \frac{\partial E}{\partial \mathbf{s}^0} \frac{\partial GR}{\partial \mathbf{W}^0} = \boldsymbol{\Phi}^0 \frac{\partial E}{\partial \mathbf{s}^0}. \quad (11)$$

3.2.1 Pre-training and dropout

In order to obtain a good initialization for joint optimization, we pre-train the network by sequential learning. As we use the dropout strategy for joint optimization, we use the gradient decent algorithm with the dropout strategy to estimate the regression coefficient matrices to solve Equations 3 and 4.

The dropout technique [10] has been shown helpful in deep neural network training, being a strong and adaptive regularizer. We adopt this technique to joint learning, which is critical to avoid over-fitting. During the forward propagation, each dimension of features $\boldsymbol{\Phi}^t$ is set to zero with probability $1 - p$. In back propagation the gradients on those dimensions are also set to zero. For local layers, the forward and backward propagation process are given by: $\mathbf{s}^t = \mathbf{s}^{t-1} + \mathbf{W}^t \mathbf{D}_z^t \boldsymbol{\Phi}^t$ and $\frac{\partial E}{\partial \mathbf{s}^{t-1}} = \frac{\partial E}{\partial \mathbf{s}^t} (\mathbf{I} + \mathbf{W}^t \mathbf{D}_z^t \boldsymbol{\Phi}^t)$, respectively. Here $\mathbf{D}_z^t = \text{diag}(\mathbf{z}) \in \mathbb{R}^{d_t \times d_t}$, diagonal elements z_i are sampled from a Bernoulli distribution $z_i \sim \text{Bernoulli}(p)$. During test, $\mathbf{W}^t \mathbf{D}_z^t$ is replaced by $p \mathbf{W}^t$. The probability p , or dropout rate, is fixed to 0.5 throughout our experiments. For the global layer, the dropout is done in a similar way.

3.2.2 Implementation details

For global features $g(I)$ we use the HOG [7] descriptor. Descriptors are computed on images down-sampled to sizes of 64×64 . Block size, block stride, cell size and number of bins are chosen as 16×16 , 16×16 , 8×8 and 9 respectively. This results in global features with 1764 dimensions. For local features $h(I, \mathbf{s})$, we use a modified version of the SIFT descriptor [15]. 128-d descriptors are extracted around each landmark, and concatenated to produce local features $\boldsymbol{\Phi} \in \mathbb{R}^{128P}$. Since the numerical approximation of $\boldsymbol{\psi}$ requires a great number of feature extraction operations and storing SIFT descriptors on all image locations requires too much memory, we modify the original SIFT descriptor so that it can be computed faster. For each image, the responses for 8 orientation bins on all locations are pre-computed and stored in 8 response maps. The Gaussian weight mask is dropped and the spatial bin interpolation is implicitly approximated by blurring the response maps using a Gaussian kernel. This is inspired by the DAISY descriptor [24]. After that the response

Table 1: Results on the LFPW and the 300-W datasets, measured by the shape error normalized by the inter-pupil distance. *The original SDM and ESR paper does not include results on the 300-W dataset and we quote results from [19].

LFPW		300-W			
Method	Normalized Error	Method	Fullset	Common Subset	Challenging Subset
CoE [1]	3.90				
ESR [3]	3.47	ESR* [3]	7.58	5.28	17.00
RCPR [2]	3.50				
SDM [25]	3.47	SDM* [25]	7.52	5.60	15.40
LBF [19]	3.35	LBF [19]	6.32	4.95	11.98
SequentialReg	3.90	SequentialReg	7.31	5.11	16.35
DeepRegLocal	3.47	DeepRegLocal	6.57	4.67	14.30
DeepReg	3.45	DeepReg	6.31	4.51	13.80

maps are converted to integral maps, where histograms can be computed with only a few addition and subtraction operations [18]. The response maps are pre-computed and stored in memory, so that the descriptors can be efficiently extracted during running time.

For both datasets, we set the number of local layers to $T = 5$. SIFT patch sizes for the first 4 local layers are set to 32×32 . The last two local layers have smaller sizes of 16×16 . We augment training samples by flipping training images horizontally. A validation set of 200 samples is split out from the training set for monitoring the training process.

The ϵ in Equation 8 is set to 2 pixels throughout our experiments. Other small values have also been tried but have no significant impact. Network parameters are updated by Stochastic Gradient Descent [13] with momentum [23] set to 0.9. The mini-batch size is set to 100. During training, the learning rate is set to 10^{-2} at first and manually decreased when validation error stops to decrease [11]. The training process is terminated when the validation error stops to decrease for enough number of iterations.

4 Experiments

4.1 Datasets and evaluation metric

Datasets: Performance is evaluated on the LFPW dataset [1] and the 300-W dataset [21]. The LFPW dataset is annotated by 29 landmarks. The dataset provides URLs only and some are no longer valid. We use 717 of the 1100 images for training and 249 of the 300 images for testing. 300-W dataset is created from several re-annotated datasets including LFPW [1], AFW [28], Helen [12] and XM2VTS [17]. The number of landmarks is 68. Since the official testing set of 300-W is not publicly available, we follow [19] and build the training set using AFW, the training set of LFPW and the training set of Helen, with 3148 images in total. Our testing set consists of IBUG, the testing set of LFPW and the testing set of Helen, with 689 images in total. Also following [19], we evaluate performance on 1) all images of the testing set, called the Fullset 2) testing sets of Helen and LFPW, called the Common Subset and 3) IBUG dataset, called the Challenging Subset.

Evaluation metric: Following [1], we evaluate performance by the average landmark error normalized by inter-pupil distance:

$$\text{error} = \frac{1}{N} \sum_{i=1}^N \frac{\frac{1}{P} \sum_{p=1}^P \sqrt{(x_p^{(i)} - \hat{x}_p^{(i)})^2 + (y_p^{(i)} - \hat{y}_p^{(i)})^2}}{d_{\text{pupils}}^{(i)}}}, \quad (12)$$

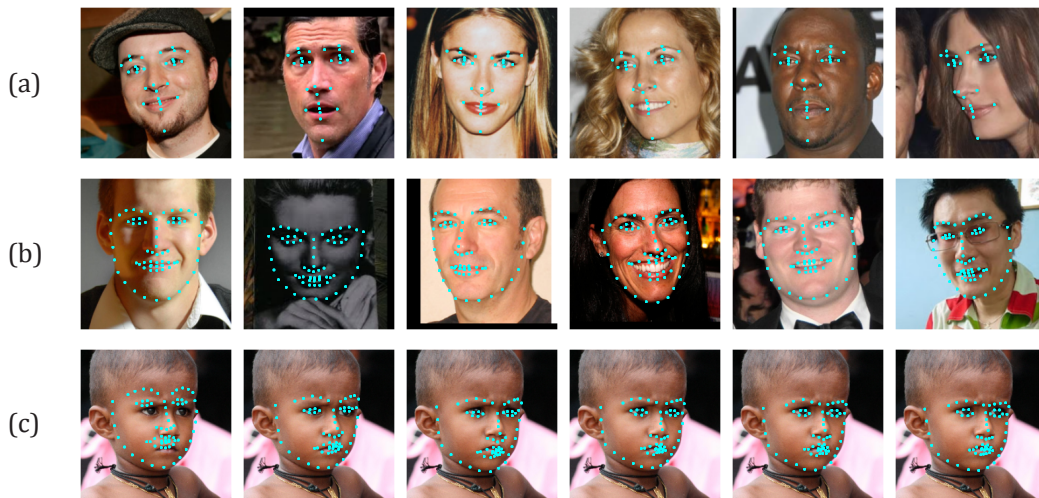


Figure 3: (a) Example results on the LFPW dataset. (b) Example results on the 300-W dataset. (c) Estimation by each stage from $t = 0$ to 5.

where $\hat{x}_p^{(i)}, \hat{y}_p^{(i)}$ are ground truth coordinates for the p -th landmark of the i -th sample, $d_{\text{pupils}}^{(i)}$ is the inter-pupil distance of the i -th sample. For 300-W, pupil landmarks are not annotated and are replaced by the mean landmarks of the landmarks around each eye.

4.2 Evaluation

We term our approach as *DeepReg*, our approach with sequential learning as *SequentialReg* and a variant of the network which drops the global regressor as *DeepRegLocal*. The initial shape estimation s^0 in *DeepRegLocal* is given by the mean shape \bar{s} calculated from the training set, as adopted in cascaded regression [25, 2, 19]. First, we compare the result of *DeepReg* with the two baseline algorithms: *SequentialReg* and *DeepRegLocal*. The results are listed in Table 1 and visualized in Figure 3.

One can see from Table 1 that *DeepReg* outperforms both *SequentialReg* and *DeepRegLocal*. The superiority over *SequentialReg* stems from joint optimization, which is able to balance the biases and the variances of all the regressors. The superiority over *DeepRegLocal* is because the global regressor is helpful to generate a robust initialization. Second, in comparison with the closely-related regression algorithm, supervised descent method (SDM, [25]), our approach performs better. The superiority of our approach and *DeepRegLocal* is not as significant as that to *SequentialReg*. The reason is that SDM did good job on feature transform, which potentially can help our approach, for example, including feature transform and even convolutions into our deep regress framework. Last, we also report the comparison results with other state-of-the-art algorithms, including the algorithm using a consensus of exemplars (CoE [1]), explicit shape regression (ESR [3]), robust cascaded pose regression (RCPR [2]) and local binary features (LBF [19]), in which our approach and LBF perform the best. As shown in Table 1, our approach performs better in 300-W Fullset and 300-W Common Subset over LBF, but poorer in LFPW and 300-W Challenging Subset. The reason is that LBF performs an extra feature learning step that is essential for good performance, and in essence our approach is able to benefit from this step if we can reproduce their reported results.

4.3 Empirical analysis

Figure 4 plots the estimation errors of all stages on the training, validation and testing sets. One can see from the plot that sequential learning tends to result in strong early stages which eliminate most of the error. The later stages, however, are much weaker. Joint learning mitigates this and the estimation gradually and evenly approaches the ground truth, resulting in a flattened error curve and better estimation eventually. Furthermore, as shown in Figure 2, joint learning balances between bias

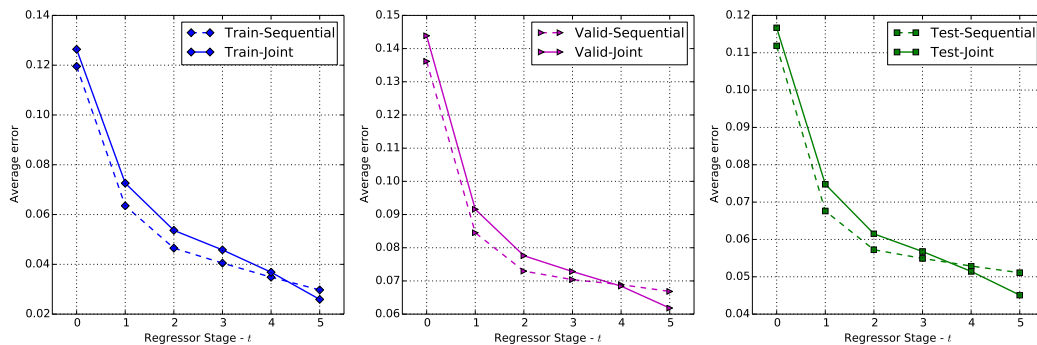


Figure 4: Average estimation error of all stages, on training, validation and testing set. Dashed line represents the sequentially trained layers and the solid line represents jointly trained layers (Tested on the 300-W dataset).

and variance and makes them gradually and simultaneously decrease, while in sequential learning the variance decreases much slower.

5 Conclusion

In this paper, we present a deep regression approach to face alignment. We adopt back-propagation with the dropout strategy to jointly optimize the regression coefficient matrices of a deep network, a sequence of one global linear regressor and multi-stage local regressors. The benefit of joint optimization lies in that the resulting regressors gradually and simultaneously decrease the bias and the variance of each shape estimator and make harmonious contributions to shape prediction, yielding a superior shape predictor over the sequential learning algorithm as done in cascaded regression. Experimental results demonstrate the powerfulness of the proposed approach.

Acknowledgements

This work was partially supported by National Natural Science Foundation of China (NSFC) (No. 61222308), and in part by NSFC (No. 61173120), Program for New Century Excellent Talents in University (No. NCET-12-0217) and Fundamental Research Funds for the Central Universities (No. HUST 2013TS115).

References

- [1] Peter N Belhumeur, David W Jacobs, D Kriegman, and Neeraj Kumar. Localizing parts of faces using a consensus of exemplars. In *Computer Vision and Pattern Recognition (CVPR), 2011 IEEE Conference on*, pages 545–552. IEEE, 2011.
- [2] Xavier P Burgos-Artizzu, Pietro Perona, and Piotr Dollár. Robust face landmark estimation under occlusion. ICCV, 2013.
- [3] Xudong Cao, Yichen Wei, Fang Wen, and Jian Sun. Face alignment by explicit shape regression. *International Journal of Computer Vision*, 107(2):177–190, 2014.
- [4] Timothy F Cootes, Gareth J Edwards, Christopher J Taylor, et al. Active appearance models. *IEEE Transactions on pattern analysis and machine intelligence*, 23(6):681–685, 2001.
- [5] Timothy F Cootes, Christopher J Taylor, David H Cooper, and Jim Graham. Active shape models-their training and application. *Computer vision and image understanding*, 61(1):38–59, 1995.
- [6] David Cristinacce and Timothy F Cootes. Boosted regression active shape models. In *BMVC*, pages 1–10, 2007.
- [7] Navneet Dalal and Bill Triggs. Histograms of oriented gradients for human detection. In *Computer Vision and Pattern Recognition, 2005. CVPR 2005. IEEE Computer Society Conference on*, volume 1, pages 886–893. IEEE, 2005.
- [8] Liya Ding and Aleix M Martinez. Precise detailed detection of faces and facial features. In *Computer Vision and Pattern Recognition, 2008. CVPR 2008. IEEE Conference on*, pages 1–7. IEEE, 2008.

- [9] Piotr Dollár, Peter Welinder, and Pietro Perona. Cascaded pose regression. In *Computer Vision and Pattern Recognition (CVPR), 2010 IEEE Conference on*, pages 1078–1085. IEEE, 2010.
- [10] Geoffrey E Hinton, Nitish Srivastava, Alex Krizhevsky, Ilya Sutskever, and Ruslan R Salakhutdinov. Improving neural networks by preventing co-adaptation of feature detectors. *arXiv preprint arXiv:1207.0580*, 2012.
- [11] Alex Krizhevsky, Ilya Sutskever, and Geoffrey E Hinton. Imagenet classification with deep convolutional neural networks. In *NIPS*, volume 1, page 4, 2012.
- [12] Vuong Le, Jonathan Brandt, Zhe Lin, Lubomir Bourdev, and Thomas S Huang. Interactive facial feature localization. In *Computer Vision–ECCV 2012*, pages 679–692. Springer, 2012.
- [13] Yann A LeCun, Léon Bottou, Genevieve B Orr, and Klaus-Robert Müller. Efficient backprop. In *Neural networks: Tricks of the trade*, pages 9–48. Springer, 2012.
- [14] Lin Liang, Rong Xiao, Fang Wen, and Jian Sun. Face alignment via component-based discriminative search. In *Computer Vision–ECCV 2008*, pages 72–85. Springer, 2008.
- [15] David G Lowe. Distinctive image features from scale-invariant keypoints. *International journal of computer vision*, 60(2):91–110, 2004.
- [16] Iain Matthews and Simon Baker. Active appearance models revisited. *International Journal of Computer Vision*, 60(2):135–164, 2004.
- [17] Kieron Messer, Jiri Matas, Josef Kittler, Juergen Luetin, and Gilbert Maitre. Xm2vtsdb: The extended m2vts database. In *Second international conference on audio and video-based biometric person authentication*, volume 964, pages 965–966. Citeseer, 1999.
- [18] Fatih Porikli. Integral histogram: A fast way to extract histograms in cartesian spaces. In *Computer Vision and Pattern Recognition, 2005. CVPR 2005. IEEE Computer Society Conference on*, volume 1, pages 829–836. IEEE, 2005.
- [19] Shaoqing Ren, Xudong Cao, Yichen Wei, and Jian Sun. Face alignment at 3000 fps via regressing local binary features. In *Computer Vision and Pattern Recognition (CVPR), 2014 IEEE Conference on*. IEEE, 2014.
- [20] David E Rumelhart, Geoffrey E Hinton, and Ronald J Williams. *Learning representations by back-propagating errors*. MIT Press, Cambridge, MA, USA, 1988.
- [21] Christos Sagonas, Georgios Tzimiropoulos, Stefanos Zafeiriou, and Maja Pantic. A semi-automatic methodology for facial landmark annotation. In *Computer Vision and Pattern Recognition Workshops (CVPRW), 2013 IEEE Conference on*, pages 896–903. IEEE, 2013.
- [22] Yi Sun, Xiaogang Wang, and Xiaoou Tang. Deep convolutional network cascade for facial point detection. In *Computer Vision and Pattern Recognition (CVPR), 2013 IEEE Conference on*, pages 3476–3483. IEEE, 2013.
- [23] Ilya Sutskever, James Martens, George Dahl, and Geoffrey Hinton. On the importance of initialization and momentum in deep learning. In *Proceedings of the 30th International Conference on Machine Learning (ICML-13)*, pages 1139–1147, 2013.
- [24] Engin Tola, Vincent Lepetit, and Pascal Fua. Daisy: An efficient dense descriptor applied to wide-baseline stereo. *Pattern Analysis and Machine Intelligence, IEEE Transactions on*, 32(5):815–830, 2010.
- [25] Xuehan Xiong and Fernando De la Torre. Supervised descent method and its applications to face alignment. In *Computer Vision and Pattern Recognition (CVPR), 2013 IEEE Conference on*, pages 532–539. IEEE, 2013.
- [26] Alan L Yuille, Peter W Hallinan, and David S Cohen. Feature extraction from faces using deformable templates. *International journal of computer vision*, 8(2):99–111, 1992.
- [27] Erjin Zhou, Haoqiang Fan, Zhimin Cao, Yuning Jiang, and Qi Yin. Extensive facial landmark localization with coarse-to-fine convolutional network cascade. In *Computer Vision Workshops (ICCVW), 2013 IEEE International Conference on*, pages 386–391. IEEE, 2013.
- [28] Xiangxin Zhu and Deva Ramanan. Face detection, pose estimation, and landmark localization in the wild. In *Computer Vision and Pattern Recognition (CVPR), 2012 IEEE Conference on*, pages 2879–2886. IEEE, 2012.